Spring 5-19-2018

Soft-Microrobotics: The Manipulation of Alginate Artificial Cells

Samuel Sheckman
Southern Methodist University, sheckel22@gmail.com

SOFT-MICROROBOTICS:

THE MANIPULATION OF ALGINATE ARTIFICIAL CELLS

Approved by:

Dr. Min Jun Kim, Ph.D.
Professor of Mechanical Engineering

Dr. Ali Beskok, Ph.D.
Professor, Department Chair of

Mechanical Engineering

Dr. Yildirim Hurmuzlu, Ph.D.
Professor of Mechanical Engineering

SOFT-MICROROBOTICS:

THE MANIPULATION OF ALGINATE ARTIFICIAL CELLS

A Dissertation Presented to the Graduate Faculty of the

Bobby B. Lyle School of Engineering

Southern Methodist University

in

Partial Fulfillment of the Requirements

for the degree of

Master of Science, Mechanical Engineering

with a

Major in Mechanical Engineering

by

Samuel Ian Sheckman

B.S., Mechanical Engineering, Drexel University

May 19, 2018

ACKNOWLEDGMENTS

This work was supported by the National Science Foundation (IIS 1734732, IIS 1712088, IIS 1619278), National Research Foundation of Korea and National Science Foundation Collaboration (OISE 1713803), Korea Evaluation Institute of Industrial Technology (KEIT) funded by the Ministry of Trade, Industry, and Energy (MOTIE)(NO. 10052980) and Open Innovation Program of NNFC (COI1710M001). Firstly, I want to thank my advisor Dr. Min Jun Kim for his guidance and tutelage over the course of my Undergraduate and Masters research at Drexel University and SMU, respectively. I would like to thank my BAST LAB colleagues Dr. Hoyeon Kim, Dr. Jamel Ali, Dr. U Kei Cheang, Louis W. Rogowski and Xiao Zhang for lending their knowledge and encouragement to complete this work. For supporting me for the NSF-NRF East Asia and Pacific Summer Institutes (EAPSI) Research Fellowship (OISE 1713803), I would like to thank Dr. Chi Won Ahn and the NNFC in Daejeon, South Korea. Additionally, I want to thank my collaborators at The University of Houston, Dr. Aaron Becker and Sheryl Manzoor for working with me over the course of time in the BAST Lab. To my Masters Committee, Dr. Ali Beskok and Dr. Yildirim Hurmuzlu, I want to thank you for taking the time to assess my work.

Sheckman, Samuel Ian B.S., Mechanical Engineering, Drexel University

Soft-Microrobotics:
The Manipulation of Alginate Artificial Cells

Advisor: Dr. Min Jun Kim, Ph.D.
Master of Science, Mechanical Engineering degree conferred May 19, 2018
Dissertation completed April 13, 2018

In this work, the approach to the manipulation of alginate artificial cell soft-microrobots, both individually and in swarms is shown. Fabrication of these artificial cells were completed through centrifugation, producing large volumes of artificial cells, encapsulated with superparamagnetic iron oxide nanoparticles; these artificial cells can be then externally stimulated by an applied magnetic field. The construction of a Permeant Magnet Stage (PMS) was produced to manipulate the artificial cells individually and in swarms. The stage functionalizes the permanent magnet in the 2D xy-plane. Once the PMS was completed, Parallel self-assembly (Object Particle Computation) using swarms of artificial cells in complex environments, controlled not by individual navigation, but by a global, external magnetic force with the same effect on each artificial cell to produce miroassemblies. A 2D grid world factory, in which all obstacles and particles are unit squares, and for each actuation, artificial cells move maximally until they collide with an obstacle or another artificial cell. Based on the design of an arbitrary 2D structure, this 2D grid world layout, will produce continuous microassemblies.

TABLE OF CONTENTS

LIST OF FIGURES

This is dedicated to my family.

Chapter 1

INTRODUCTION

Microrobotics is a growing and advancing concentration in the field of robotics and engineering. As the interdisciplinary nature of the research allows an interaction between mechanical, electrical and materials engineering with medicine and outward research fields, the concentration is on the vanguard of science. Within the robotics research field, there is the discipline of soft-robotics, naturally derived materials are used to mimic natural design and create a robot to be used in situations where rigid mechanical structures would not be capable [25, 54].

Microrobotics has also been introduced to this new soft-material mechanism to perform specific tasks. As such, microrobotics can be characterized as three forms of robots with rigid-particles, soft-particles, and biological hybrids. Work over the past few decades have shown that these particle microrobots can be manufactured with large populations (10^3-10^{14}) of small scale (10^{-9}-10^{-6} m) robots using diverse array of materials and techniques [14,32,38]. Since these microrobots are so small, they are ideal for several invasive medical procedures; such as, but not limited to: minimally invasive surgery, targeted therapy, disease diagnosis, single-cell manipulation and tissue engineering [1, 7, 48, 57, 58]. These microrobots are wireless controlled through external stimulis [12, 15, 17, 18, 21, 32, 55], and have been shown to complete specific tasks [28]. Since microrobots are on the micro-scale this provides a unique challenge to control; as limits in fabrication do not allow for or have little-to-no onboard computing or communication ability [12, 14, 18]. These limitations make controlling swarms of these robots individually impractical. Thus, these robotic systems are often controlled by a global external signal (e.g. chemical gradients, electric and magnetic fields), which makes motion planning for large robotic populations in tortuous environments difficult. Having

only one global signal that simultaneously affects all robots at once limits the swarms ability to perform complex operations. Independent control is possible by designing heterogeneous particles that respond differently to the global input, but this approach requires precise differences in each robot and is best suited for small populations. Alternatively, control symmetry can be broken using interactions between the robot swarm and obstacles in the environment [4, 5].

Naturally derived polysaccharide based hydrogels have presented themselves as the ideal soft-microrobot. Their biocompatibility, hydrophilicity, as well as the ability to reversibly encapsulate organic and inorganic materials has shown the capability of the material. Once material is encapsulated into a hydrogel, the droplets mimic the basic structure of living cells (membrane, cytoplasm, organelles, etc.), and as such is also referred to as an *artificial cell* [8, 9, 34]. Fabricated through the process of crosslinking alginate sodium when in the presence of divalent cations, most effectively with barium and calcium. As an over exposure to former is toxic to nearly all living cells, calcium is the preferred method of crosslinking [29]. Over time the outer polymer bilayer of the artificial cell begins to become more porous, the internal payload is naturally released and the artificial cell reaches the end of its usefulness. As a result, coating of the outer surface can result in the polymer layer to become more stable, prolonging the viability of the particle. These coated particles result in higher viability in both *ex vivo* and *in vivo* environments. These outer polymer layer is also reactive the pH of the surrounding medium, release of encapsulated materials and change in size occurs more rapidly. Coating agents strengthen the ionic strength of the outer polymer layer allowing the extension of the artificial cells life [30, 41–43]. Without a coated layer, there is still great effect temperature and pH has on the shape and rigidity of artificial cells. Under atmosphere conditions, room temperature and neutral pH, particles remain similar size throughout experimentation [50]. Additionally, hydrogels capibilies of encapulation enables the facilitation to fabricate biosensing soft-microrobots for biomedical purposes [53].

Single bead particles on the microscale are typically reserved for boundary surface motion applications. The motions are characterized into two subsets, rolling motion and translational (dragging) motion, depending on the external stimulation that is experienced by the particle. Purcells Scallop Theorem states that a reciprocating motion, such as a scallop opening and closing its simple hinged shell, would not be sufficient to create migration at low Reynolds number [35]. As such, a single symmetric magnetic bead, far from boundaries, under a rotating externally applied magnetic field, will stay in the same location. A multi-bead structure, of at least three particles, breaks the symmetry and due to its achirality can move with a swimming motion through the media under a rotating magnetic field [10]. Thus, a single symmetric particle structure is typically manipulated using either a statically applied magnetic field or magnetic gradient in Newtonian conditions [37]. Alginate hydrogels has been shown to both encapsulate and ionically bond flagellar bodies. The flagella bonded to the surface, produce a nonreciprocating motion while swimming through a medium at low Reynolds number, are then manipulated for the purpose of locomotion of the microrobot [33].

To control the manipulation of these artificial cells, the design and fabrication of an alternative magnetic stimulation was sought to increase working area with decrease cost factors. As mentioned prior, typical actuation of single particles are broken in two subsets, these motions require external magnetic stimuli for these moving motions can be controlled using an external rotating magnetic field from a Helmholtz coil system or a magnetic gradient by a Maxwell coil system [2,11,32]. These coil systems are expensive and cumbersome to set up as the power supplies can cost tens of thousands of dollars. These systems are limited by the current the power supplies can generate and the heating effect of the working area that is caused due by the heating of the copper wires. Producing a system that can produce an externally applied magnetic field and have an enlarged working area introduced the concept of a Permanent Magnet Stage. Instead of a high-power system, a permanent magnetic would be used to drag the microrobots and alginate artificial cells to their desired destinations. This system is designed to have interchangeable magnetics as to allow different magnetic field

types and strengths to be used for specific applications. Research groups have conducted similar research into permanent magnetic manipulation to maneuver particles [24,39]. These systems are much more elaborate and would require more setup and cost. With this system, a single global input can control the microrobotic artificial cells. The ability to manipulate a single particle and a swarm of particles is therefore possible under these conditions.

To further the application of microrobotics, a long-sought foundation towards the creation of complex microassemblies has been needed. With the introduction of object particle computation, multiple microrobots can be manipulated in unison by a single external input and directed to different locations [4, 5]. Typical fabrication of multiple microassemblies requires the use of continual microfabrication techniques which increases the initial costs of fabrication. To decrease this effect, object particle computation allows for a single design to be constructed using traditional and nontraditional microfabrication techniques to manufacture a specific design to fabricate parallel microassemblies continuously. To produce constructions with microgels, groups have traditionally turned to non-robotic microfluidic systems that utilize a variety of actuation methods, including mechanical, optical, dielectrophoretic, acoustophoretic, and thermophoretic [3, 13, 16, 47, 56]. While each of these methods has proven to be capable of manipulating biological cells, each method has significant drawbacks that limit their widespread application. For example, microscale mechanical, acoustophoretic, and thermophoretic manipulation methods use stimuli that can be potentially lethal to live cells [23]. Furthermore, most, if not all, of these techniques require expensive equipment and lack control schemes necessary to precisely manipulate large numbers of cells autonomously [45,51,52]. Obstacles present in the workspace can *deterministically* break the symmetry of approximately identical robotic swarms, enabling positional configuration of robots [6], while using biologically compatible magnetic stimulus. Given sufficient free space, a single obstacle is sufficient for positional control over N particles. This method can be used to form complex assemblies out of large swarms of mobile microrobotic building blocks, using only a single global input signal. This algorithm uses path

planning techniques described in [36, 49]. Using these techniques this methodology can be used towards the development of drug delivery and tissue engineering applications.

This manuscript follows the following outline: 1) Introduction, 2) Methods, background in artificial cell fabrication, design and fabrication of the Permanent Magnet Stage (PMS) Controller, theory of the object particle computation, and experimental setup, 3) Experimental Results, and 4) Discussion and Future work.

Chapter 2

MATERIALS AND METHODS

2.1. Alginate Artifical Cell Preparation

The primary microrobot during experimentation is the artifical cells produced from alginate hydrogels. The formation of the hydrogel is caused by a crosslinking process between Alginate-Na and Calcium Chloride [29]; other crosslinking agents are available, but calcium is the only one that is not harmful to the body. The encapsulated the payload can be released using chelating agents, most prominently ethylenediaminetetraacetic acid (EDTA). Using solutions of Sodium Alginate interacting with Calcium Chloride, the artificial cells predominately in most experiments with the encapulsation of iron oxide paramagnetic nanoparticles. Paramagnetic nanoparticles are encapsulated to allow for steerable propulsion.

2.2. Pressure Driven Fabrication Method

To fabricate alginate artificial cells on the macro-scale, a purely pressure driven method of manufacturing is deployed. Typically, the use of a pipette is typical for this type of fabrication, due to the ease of use and wide availability. Pipettes follow the capillary principles of fluid mechanics and as such, the size of the particle is expressed by the Young-Laplace equation [40]. The Young-Laplace equation is as follows:

$$\Delta P = 2\sigma_p[\frac{1}{R_d} - \frac{1}{R_p}] \tag{2.1}$$

where ΔP, σ_p, R_d, and R_p, are the change in pressure, surface tension of the alginate solution, radius of the alginate particle, and the radius of the pipette, respectively. Depending on the change in pressure, the size of the particle will alter. Thus, the use of pipettes will produce alginate artifical cells, but results are be scattered due to human error and input of pressure into the pipette tip. This method can produce large scale millimeter alginate artificial cells, when large scale as shown in figure 2.1 below. Figure 2.1 shows the pipette process as well as a millimeter-scale alginate microrobot.

Figure 2.1. a) Pressue Driven Pipette Process. A concentration of Alginate-Na is mixed with superparagmanetic iron oxide nanoparticles and in side of the pipette tip. Pressure is then place on the pipette to produce droplets of the particles of the desired size into a Calcium Cloride bath. Crosslinking process is instantaneous. (Image Courtesy of Dr. Jamel Ali) b) A millimeter scale artifical cell, produced via Pressure Driven Method. Scale bar is 1mm.

Additionally, this pressure driven method can produce droplets using a Bio 3D-printer. Due to recent advances in 3D printing and the expiring of patents in late 2000's, the 3D printing industry has exploded. Most recently, the biggest advancements have been in the field of biological 3D-printers. Typically, these systems use sryinges to change resolution, extrusion based bioprinting produced from a pnumatic valve system allows for consistant particle droplets to be formed [44]. These however are more tear shaped to surface tension

from the nozzle. A typical cylindrical needle gage will require approximatley 180-190 kPa to produce a single droplet, where as use of a conical needle gage will drastically reduce the applied pressure to approximately 10-15 kPa. Our lab currently possess a Cellink Inkredible+ 3D-BioPrinter, this system can be seen in figure 2.2.

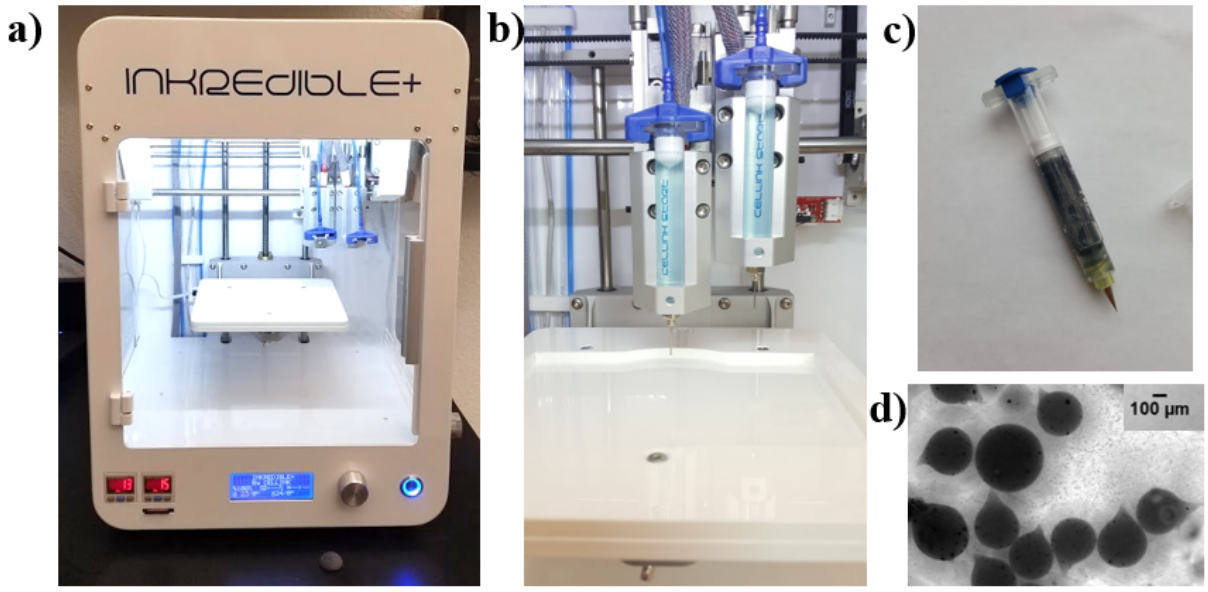

Figure 2.2. 3D-BioPrinter Process. a) The Cellink Incredible+ with current pressue application in the lower left corner, pressue is read in kPa. b) Duel syringe set-up displayed, the current needle gage 20. c) A Cellink Sryinge with Alginate-Na filled and a 100μm diameter conical needle before placed inside the Inkredible+ for droplet manufacturing. d) Alginate Artifical Cells after fabricated through 3D-Biprinter process, scale bar is 100μm

2.3. Centrifugal Fabrication Method

The use of the centrifugal method produces Alginate artifical cells on the scale of 500μm to 80μm, as shown through experiemental results in figure 2.3(a). To determine the size of the final particle the following governing equation used [2], and thus explained as:

$$d_p = \sqrt[3]{\frac{6 d_n \sigma_p}{\rho_p g}} \tag{2.2}$$

where d_n, σ_p, ρ_p, and g, are the diameter of the nozzle, surface tension of the alginate solution, density of alginate solution, and the applied gravitational force, respectively. The surface tension of alginate is 65.46 mN/m [20], and a density of 1.1 g/cm^3.

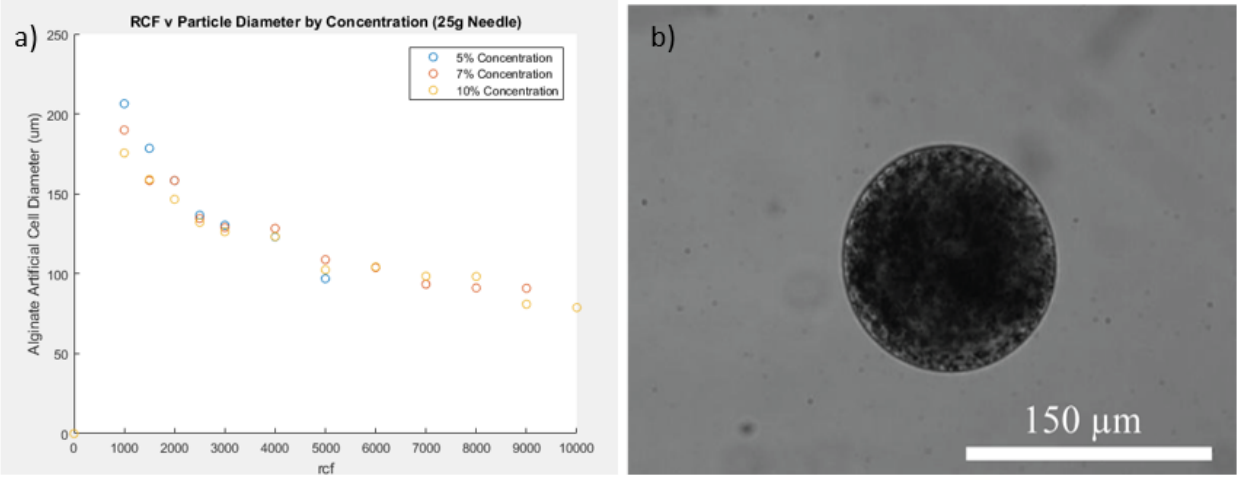

Figure 2.3. Alginate Artifical Cell Fabrication results. a) Average particle size after changing concentration. b) 150μm Alginate Artifical Cell under 1500 rcf and a 27g needle [46]

To conduct the fabrication of artificial cells with this method, a microcentrifuge is used. The change in relative centrifugal force (rcf) is the acceleration in a centrifuge normalized to Earths gravity. This rcf value is correlated to the size of the needle diameter producing the artificial cells. The higher the rcf being applied, the smaller the artificial cell, this is however limited by the gage size of the needle. Large needle gages such as 25g will produce larger particles at 1000 rcf compared to a 30g needle under the same conditions. Particle size can be drastically decreased, this can also be seen in the change in concentration of Alginate-Na being used in crosslinking. The higher the concentration, the smaller the overall size of the particle under similar conditions. The consistency of the centrifugal method is its advantage

over the pressure driven method, using equation 2.2 an alginate artificial cell of reasonable diameter can be fabricated.

The process to produce these artificial cells is as follows: 1) Using a 1.5ml microcentrifuge tube, punch a hole approximately the size of the diameter of the needle gage required for fabrication in the center of the tube cap. 2) After thoroughly cleaning the microcentrifuge tube of debris, place the desired concentration of Calcium Chloride approximately 0.1-0.2ml below the tip of the needle. The needle must not touch the as the crosslinking of Alginate-Na and Calcium Chloride is nearly instantaneous reaction once there is contact. 3) Enter the desired concentration of Alginate-Na in the cap of the needle. Finally, 4) Place the microcentrifuge tube into a microcentrifuge with counter weight and enter the desired rcf. These steps result in the mass fabrication of alginate artificial cells, with the encapsulation of a stimulating material such as iron oxide, controllability is achievable when placed under an externally applied magnetic field.

The average particle size during experimentation is approximately 300 μm, and were composed of a concentration of 5 percent (w/v) Alginate-Na and 5 percent (w/v) concentration of $CaCl_2$, and then encapsulated with 10 percent (w/v) superparamagnetic nanoparticles (Iron oxide, Sigma-Aldrich). Using a 27g needle and 300 rcf.

2.4. Permanent Magnet Stage (PMS) Design

The proposed permanent magnet stage controller would allow for interchangeable permanent magnets. This parameter of design became of utmost importance, as different application would require a different magnetic field. Depending on the size of the magnet field, the Field of play needs to be large enough so when the magnet is not being used, it would not interfere with any microrobot shown in the field of view. Field of play, as we have termed it, describes the total accolated space the magnet can move in the xy-plane. The total space

in the field of play, is 12 x 24 cm^2. The field of view, displayed through a microscope allows for movement to viewed and physically analyzed. Typically, the field of view is in the center of the field of play, which allows for the magnet to safely exit any time the magnetic field is needed on the environment.

An additional parameter of the design was that the stage must work on an inverted microscope and a stereoscopic microscope. This would allow for a smaller and smaller field of view and smaller microrobots to be investigated; as inverted microscopes allow for interchangeable optics to be used, generating greater magnification than that of traditional stereoscopic microscopes. As such, there were some imitations to the size of the stage. Using a Olympus IX50 inverted microscope as the basis for the stage dimensions, the overall length of the stage comes to be 22.86 x 35.56 cm^2. The height of the stage is 15.24 cm, from the base of to the top of the z-axis. The figure below shows the CAD model of the stage, as it would be used under a stereoscopic microscope.

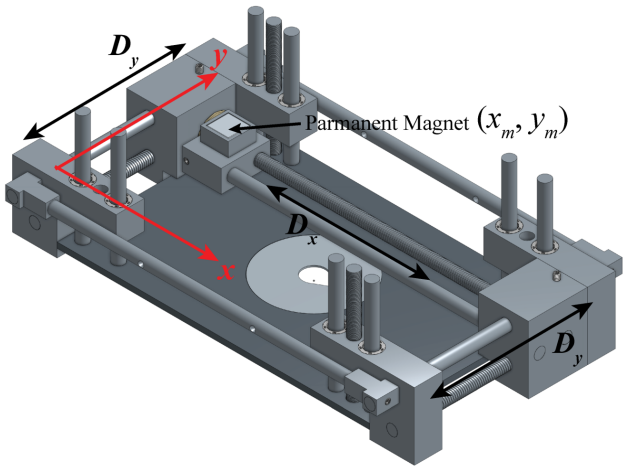

Figure 2.4. CAD Model of PMS [46]

Raw material for the stage was 6061 T-6 Aluminum (McMaster-Carr, Atlanta Ga, USA). The base is a 1.27 cm thick polycarbonate sheet. Stepper motor holders were designed in

CAD and printed by using 3D printer. A seperate adjustable stage, from Edmund Optics, is used to reduce vibration from the movement of the permanent magnet.

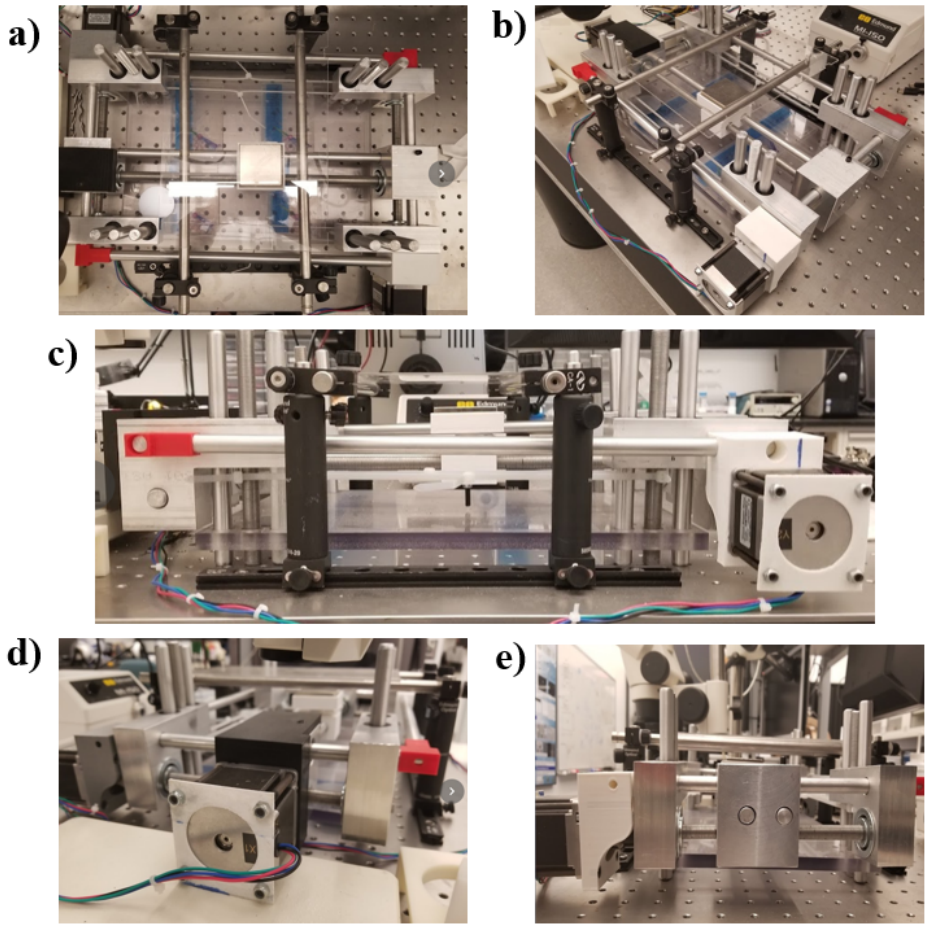

Figure 2.5. Final Assembly of the PMS. a) Top View. b) Isometric View. c) Front View. d) Left View. e) Right View.

Using an Ardunio R3, two BigEasy Stepper Motor Drivers, and three stepper motors (Sparkfun.com); the stage was controlled through a designed graphic user interface (GUI) by way of a C++ program. Using programmed C++, it allows giving the control input signal to the Ardunio R3 by USB communication during the sampling time of 0.5 s. Then, the Ardunio R3 generates the digital signal to BigEay Stepper Motor Drivers in terms of the direction and the turn of steps. Stepper Motor Drivers controls the stepper Motors to

follow the desired input rotation with a maximum acceleration.

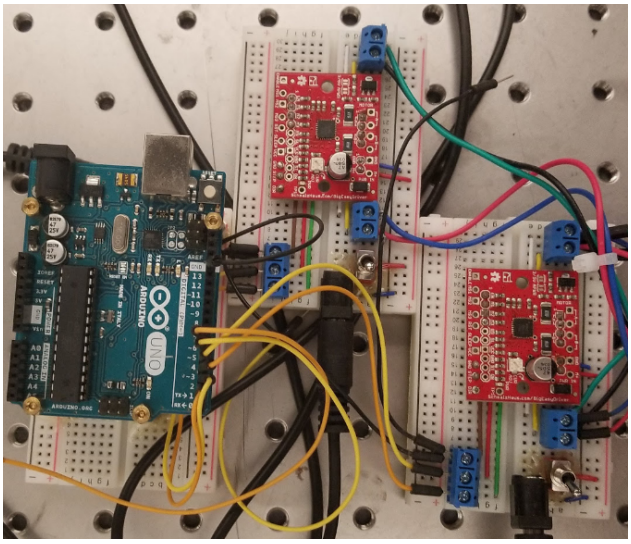

Figure 2.6. Ardunio Controller. Two BigEasy Stepper Motor Drivers are used and connected through breadboards to the stepper motors.

Each input was manually entered into the C++ based GUI, then, the magnetic would move as a continuous function, or in single steps. The time step of the movement was shortened to very small value to allow the magnetic particles to move across the field of view. If the magnet moved to quickly, the particles would not react to magnetic field. A balance between speed and strength of the magnet needed to be found in this open-loop system.

2.5. Permanent Magnet Stage (PMS) Governing Forces

Governing the controlling system is the permanent magnet, distributing the magnetic field upon which the microrobots are being manipulated. As described in [19, 31], using the equation for magnetic flux density of a permanent magnet can be found as:

$$\mathbf{B} = \mu_0(\mathbf{H} + \mathbf{M}) \tag{2.3}$$

where, μ_0, H and M are the permeability of free space, the magnetic field and the magnetization produced by the permanent magnet, respectively. The value for μ_0 is $1.256x10^{-6}H/m$. Further analysis can be performed to find the magnetic force being exerted by the permanent magnet and displayed on the magnetic dipole moment $\mathbf{m}$.

$$F_m = \nabla(U) = \nabla(\mathbf{m} \cdot \mathbf{B}) = (\nabla\mathbf{m}) \cdot \mathbf{B} + \mathbf{m} \cdot \mathbf{B} = (\mathbf{m} \cdot \nabla)\mathbf{B} \tag{2.4}$$

where U represents the gradient of the magnetic dipole energy. Since the alginate microrobots encapsulate paramagnetic nanoparticles and the microrobots are in a non-magnetic fluid, therefore $m = V\mathbf{M} = VH$. From equations (2.3) and (2.4), as well knowing the relationship of $(1+\chi)$ as the relative permeability of the media, represented by μ_r; the force can be rewritten as:

$$F_m = \frac{V\chi}{\mu_0\mu_r}(\mathbf{B} \cdot \nabla)\mathbf{B} \tag{2.5}$$

where V and χ is the volume of an alginate microrobot and the effective magnetic susceptibility, respectively. The fluid medium in experiments is a solution of Deionized water and tween 20, this solution is shows no magnetic properties. Thus, the effective susceptibility of the medium is assumed to be 1.

The magnet used in the experiments was a NdFeB, Grade N42/N52 (KJ Magnetics, Pipersville PA, USA). For the N42 magnet, the size was 5.08 x 5.08 cm^2, with a thickness of 0.635 cm. The N52 magnet size was 2.54 x 2.54 cm^2, with a thickness of 1.27 cm. For design

a large magnet was used to determine space, the N52 was used more in experimentation. The FEMM analysis of both magnets are shown below in figure 2.7.

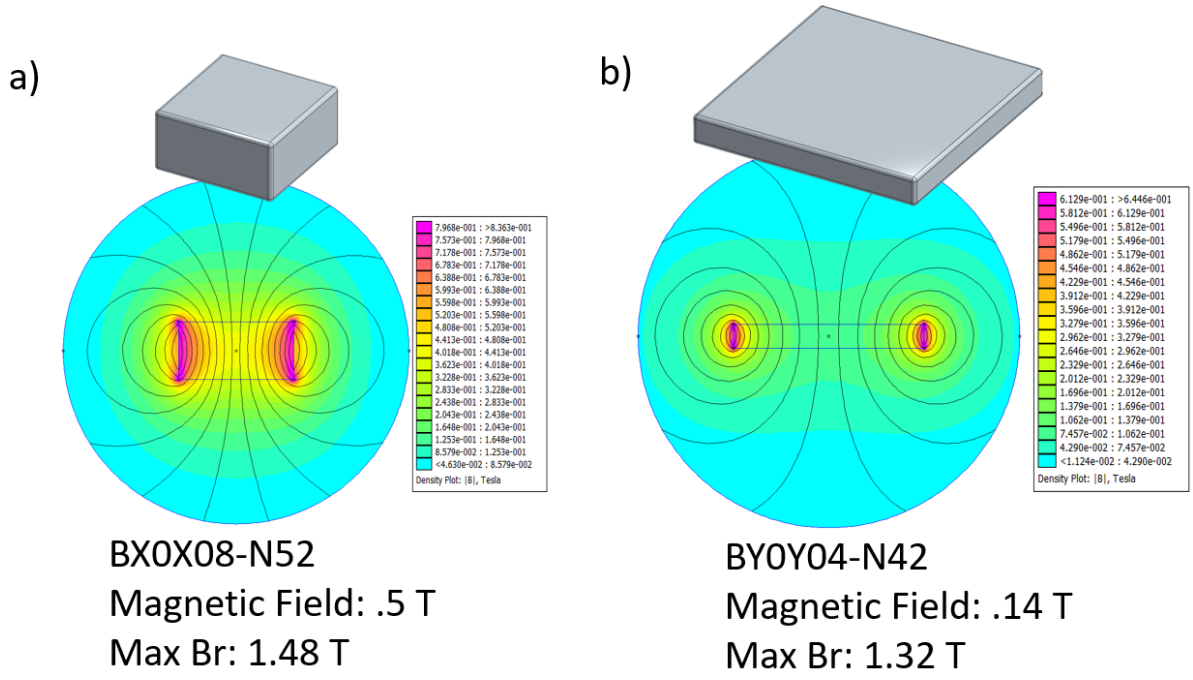

Figure 2.7. FEMM analysis of Permanent Magnets. a) N52 NdFeB magnet b) N42 NdFeB magent.

These are not the only forces governing the microrobots, drag forces to be considered. At the small scale, forces such as gravity can be neglected and forces viscous forces become more of an obstacle to overcome. For this reason, the drag the microrobots are experiencing needs to be calculated in the total force equation. The drag force of a microrobot at low Reynolds Number [22], can be written as:

$$F_d = 6\pi\mu \mathbf{v} R \tag{2.6}$$

where V, R, and μ are defined as the velocity, radius of the microrobot, and the viscosity of the fluid, respectively. Since the fluid is remaining still in our case, the velocity is that experience by the microrobot. When combining Eq. (2.5) and Eq. (2.6), the equation for the total force experienced by a microrobot to be:

$$F_m = \frac{V\chi}{\mu_0\mu_r}(\mathbf{B}\cdot\nabla)\mathbf{B} - 6\pi\mu\mathbf{v}R \tag{2.7}$$

2.6. Object Particle Computation

Through the use of obstacle laden environment, where artificial cells or microrobots, move through a maze like structure to reach a final destination. In this algorithmic procedure, alginate artifical cells are hereby termed polyominoes, to describe the arbitary 2D geometric figure by the joining one or more equal 'squares' edge to edge [27]. The maze is designed to interact with the particles to create pre-determined complexes at the end result. A swarm of microrobots are controlled using a global input and move until an obstacle stopped them from moving any further. Particle computation uses logic gates and wiring gates to move and connect the microrobots from stage one to final assembly [5]. From rules of object particle computation, an obstacle laden environment can be determined and a *Model* can be expressed as [4, 5]:

1. A 2D workspace is filled with a number of unit-square particle and some fixed unit-square blocks. Each unit square in the works space is either free, which a robot can occupy or obstacle which a particle may not occupy.

2. All particles are commanded in unison: the valid commands are Go Up (u), Go Right (r), Go Down (d), Go Left (l).

3. The particles all move in the commanded direction until the hit an obstacle or a stationary robot.

The polyominoes will continue to move in the commands given, until the final assembly is created. Further development of these laws to produce individual factories to manufacture parallel microassemblies of nearly any shape desired is expressed in Manzoor et al. [27], and shown here in this section. These algorithms described in this section were developed at The University of Houston in collaboration with Dr. Aaron Becker and Sheryl Manzoor, the matlab code of these algorithms can be found at [26].

Arbitary 2D Shapes Require Two Particle Species

Polyominoes have four-point connectivity: a 4-connected square is a neighbor to every square that shares an edge with it.

Lemma 1: Any polyomino can be constructed using just two species

Proof: Label a gridwith an alternating pattern like a checkerboard. Any desired polyomino can be constructed on this checkerboard, and all joints are between dissimilar species. An example shape is shown in Fig. 2.8. Red and blue colors are used to indicate particles of different species.

The sufficiency of two species to construct any shape gives many options for implementation. The two species could correspond to any gendered connection, including ionic charge, magnetic polarity, or hook-and-loop type fasteners. Large populations of these two species can then be stored in separate hoppers and, like two-part epoxy, only assemble when dissimilar particles come in contact.

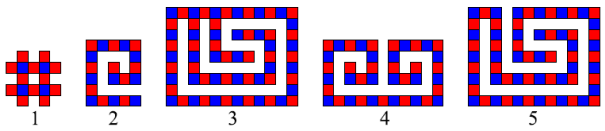

Figure 2.8. Polyomino Parts. Assembly difficulty increases from left to right [27].

Complexity Handled in This Paper

2D part geometries vary in difficulty. Fig. 2.8 shows parts with increasing complexity. Label the first particle in the assembly process the seed particle. Part 1 is shaped as a # symbol. Though it has an interior hole, any of the 16 particles could serve as the seed particle, and the shape could be constructed around it. The second shape is a spiral, and must be constructed from the inside-out. If the outer spiral was completed first, there would be no path to add particles to finish the interior because added particles would have to slide past compatible particles. Increasing the number of species would not solve this problem, because there is a narrow passage through the spiral that forces incoming parts to slide past the edges of all the bonded particles. The third shape contains a loop, and the interior must be finished before the loop is closed. Shape 4 is the combination of a left-handed and a right-handed spiral. Adding one particle at a time in 2D cannot assemble this part, because each spiral must be constructed from the inside-out. Instead, this part must be divided into subassemblies that are each constructed, and then combined. Shape 5 contains compound overhangs, and may be impossible to construct with additive 2D manufacturing using only two species. The algorithms in this letter detect if the desired shape can be constructed one particle at a time. If so, a build order is provided, and a factory layout is designed.

Discovering a Build Path

Given a polyomino, Alg. 1 determines if the polyomino can be built by adding one component at a time. The problem of determining a build order is difficult because there are $O(n!)$ possible build orders, and many of them may violate the constraints shown in the rules established previously. Each new tile must have a straight-line path to its goal position in the polyomino that does not collide with any other tile, does not slide past an opposite specie tile, and terminates in a mating configuration with an opposite specie tile. However, as in many robotics problems, the inverse problem of deconstruction is easier than the forward problem of construction.

Algorithm 1: FINDBUILDPATH($\mathbf{P}$).

$\mathbf{P}$ is the x, y coordinates of a 4-connected polyomino. Returns $\mathbf{C}$, $\mathbf{c}$ and $\mathbf{m}$ where $\mathbf{C}$ contains sequence of polyomino coordinates, $\mathbf{c}$ is a vector of color labels, and $\mathbf{m}$ is a vector of directions for assembly.

1: $\mathbf{c} \leftarrow$ LABELCOLOR($\mathbf{P}$)
2: $\{\mathbf{C}, \mathbf{m}\} =$ DECOMPOSE $(\mathbf{P}, \mathbf{c})$
3: **return** $\{\mathbf{C}, \mathbf{c}, \mathbf{m}\}$

Figure 2.9. Algorithm 1: Finding the Build Path [27].

Alg. 1 first assigns each tile in the polyomino a color, then calls the recursive function DECOMPOSE, which returns either a build order of polyomino coordinates and the directions to build, or an empty list if the part cannot be constructed. DECOMPOSE starts by calling the function ERODE. ERODE first counts the number of components in the 8-connected freespace. An 8-connected square is a neighbor to every square that shares an edge or vertex with it. If there is more than one connected component, the polyomino contains loops. ERODE maintains an array of the remaining tiles in the polyomino $\mathbf{R}$. In the inner *for loop* at line 2, a temporary array $\mathbf{T}$ is generated that contains all but the jth tile in $\mathbf{R}$ sorted by the number of neighbors so a tile with one neighbor is checked before tiles with two or three. This *for loop* simply checks (1) if the jth tile can be removed along a straight-line path without colliding with any other particle or sliding past an opposite specie

tile in line 2, (2) that its removal does not fragment the remaining polyomino into more than one piece in line 2, and (3) that its removal does not break a loop in line 2. If no loops are present, this algorithm requires at most $n/2(1+n)$ iterations, because there are n particles to remove, and each iteration considers one less particle than the previous iteration.

Algorithm 2: ERODE($\mathbf{P}, \mathbf{c}$).

$\mathbf{P}$ is the x, y coordinates of a 4-connected polyomino and $\mathbf{c}$ is a vector of color labels. Returns $\mathbf{R}$, $\mathbf{C}$, $\mathbf{m}$, and ℓ where $\mathbf{R}$ is a list of coordinates of the remaining polyomino, $\mathbf{C}$ contains sequence of tile coordinates that were removed, $\mathbf{m}$ is a vector of directions for assembly, and ℓ if loops were encountered. $\mathbf{d} \leftarrow \{r, d, l, u\}$

1: $\mathbf{C} \leftarrow \{\}, \mathbf{m} \leftarrow \{\}, \ell \leftarrow$ FALSE, $\mathbf{R} \leftarrow \mathbf{P}$
2: $w \leftarrow |8\text{-CONNCOMP}(\neg \mathbf{R})|$
3: **while** $1 < |\mathbf{R}|$ **do**
4: *successRemove* $\leftarrow$ FALSE
5: $\mathbf{R} \leftarrow$ SORT($\mathbf{R}$) ▷ sort by number of neighbors
6: **for** $j \leftarrow 1, j \leq |\mathbf{R}|$ **do**
7: $\mathbf{p} \leftarrow \mathbf{R}_j, \mathbf{T} \leftarrow \mathbf{R} \backslash \mathbf{R}_j$
8: **for** $k \leftarrow 1, k \leq 4$ **do**
9: **if** CHECKPATHTILE($\mathbf{T}, \mathbf{p}, \mathbf{d}_k, \mathbf{c}$) **and**
10: $1 = |4\text{-CONNCOMP}(\mathbf{T})|$ **then**
11: **if** $w = |8\text{-CONNCOMP}(\neg \mathbf{T})|$ **then**
12: $\mathbf{R} \leftarrow \mathbf{T}$, *successRemove* $\leftarrow$ TRUE
13: $\mathbf{C}_{1+|\mathbf{R}|} \leftarrow \mathbf{p}, \mathbf{m}_{|\mathbf{R}|} \leftarrow \mathbf{d}_k$
14: **else** $\ell \leftarrow$ TRUE
15: **break**
16: **if** *successRemove* = FALSE **then**
17: $\mathbf{C} \leftarrow \{\}, \mathbf{m} \leftarrow \{\}$
18: **break**
19: **if** $|\mathbf{R}| = 1$**then**
20: $\mathbf{C}_1 \leftarrow \mathbf{R}_1$
21: **return** $\{\mathbf{R}, \mathbf{C}, \mathbf{m}, \ell\}$

Figure 2.10. Algorithm 2: ERODE [27].

Polyominoes with loops require care, because decomposing them in the wrong order can make disassembly impossible, as shown in 2.12a. If loops exist then ERODE may return only a partial decomposition, so DECOMPOSE must then try every possible break point and recursively call DECOMPOSE until either a solution is found, or all possible decomposition orders have been tested. The worst-case number of function calls of DECOMPOSE are proportional to the factorial of the number of loops, O (|8-CONNCOMP($\neg$ **P**)|!). Though

large, this is much less than $O(\ n!)$.

Algorithm 3: DECOMPOSE($\mathbf{P}, \mathbf{c}$).

$\mathbf{P}$ is the x, y coordinates of a 4-connected polyomino and $\mathbf{c}$ is a vector of color labels. Returns $\mathbf{C}$ and $\mathbf{m}$ where $\mathbf{C}$ contains sequence of polyomino coordinates and $\mathbf{m}$ is a vector of directions for assembly. $\mathbf{d} \leftarrow \{u, d, l, r\}$

```
{R, C, m, ℓ} ← ERODE (P, c)
if |R| = 0 or ¬ℓ then
    return {C, m}
for j ← 1, j ≤ |R| do
    p ← R_j, T ← R\R_j
    for k ← 1, k ≤ 4 do
        if ( CHECKPATHTILE(T, p, d_k, c) and
             1 = |4-CONNCOMP(T)|) then
            {C2, m2} ← DECOMPOSE (T, c)
            if C2 ≠ {} then
                C_{1:|C2|+1} ← {C2, p}
                m_{1:|m2|+1} ← {m2, d_k}
                return {C, m}
            break
return {C ← {}, m ← {}}
```

Figure 2.11. Algorithm 3: DECOMPOSE [27].

Hopper Construction

Two-part adhesives react when components mix. Placing components in separate containers prevents mixing. Similarly, storing many particles of a single species in separate containers allows controlled mixing. We can design *part hoppers*, containers that store similarly labelled particles. These particles will not bond with each other. The hopper shown in 2.12b releases one particle every cycle. Delay blocks are used to ensure the nth part hopper does not start releasing particles until cycle n. For ease of exposition, this letter has a unique hopper for each tile position. This enables precise positioning of different materials, but a particle logic system could use just two hoppers, similar to our particle logic systems in [5].

Part Assembly Jigs

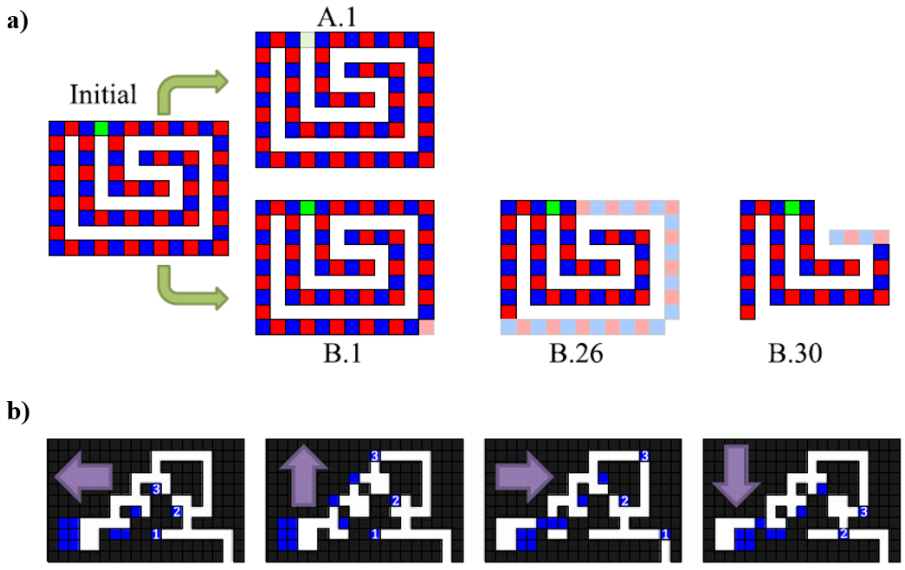

Figure 2.12. a) Deconstruction order matters if loops are present. Loops occur when the 8-connected freespace has more than one connected component. In the top row the green tile is removed first, resulting in a polyomino that cannot be decomposed. However, if the bottom right tile is removed first, deconstruction is possible. b) Hopper with five delays. The hopper is filled with similarly-labelled robots that will not combine. Every clockwise command cycle releases one robot from the hopper. [27]

Assembly is an iterative procedure. A factory layout is generated by BUILDFACTORY($\mathbf{P}$,n_c), described in Alg. 4. This function takes a 2D polyomino $\mathbf{P}$ and, if $\mathbf{P}$ has a valid build path, designs an obstacle layout to generate n_c copies of the polyomino. A polyomino is composed of $|\mathbf{P}| = n$ tiles. For each tile, the function FACTORYADDTILE (n_c , $\mathbf{b}$,m,C,c,w) described in Alg. 5 is called to generate an obstacle configuration $\mathbf{A}$. $\mathbf{A}$ forms a hopper that releases a particle each iteration and a chamber that temporarily holds the partially assembled polyomino $\mathbf{b}$ and guides the new particle C to the correct mating position.

Algorithm 4: BUILDFACTORY($\mathbf{P}, n_c$).

$\mathbf{P}$ is the x, y coordinates of a 4-connected polyomino. n_c is the number of parts desired. Returns a two dimensional array $\mathbf{F}$ containing the factory obstacles and filled hoppers.

1: $\mathbf{F} \leftarrow \{\}$ ▷ the factory obstacle array
2: $\{\mathbf{C}, \mathbf{c}, \mathbf{m}\} \leftarrow$ FINDBUILDPATH($\mathbf{P}$)
3: **if** $\{\} = \mathbf{m}$ **then**
4: **return** $\mathbf{F}$
5: $\{\mathbf{A}, \mathbf{b}\} \leftarrow$ FACTORYFIRSTTILE $(n_c, \mathbf{c}_i, w)$
6: **for** $i \leftarrow 2, i \leq |\mathbf{c}|)$ **do**
7: $\{\mathbf{A}, \mathbf{b}\} \leftarrow$ FACTORYADDTILE $(n_c, \mathbf{b}, \mathbf{m}_{i-1}, \mathbf{C}_i, \mathbf{c}_i, w)$
8: $\mathbf{F} \leftarrow$ CONCATFACTORIES $(\mathbf{F}, \mathbf{A})$
9: **return** $\mathbf{F}$

Figure 2.13. Algorithm 4: Finding the Build Path [27].

Analysis

Once the algorithms have been processes for specific polyomino buildfactory, these algorithms need to be analyzed to give approximate simulations. These are processed by calculating the *Maximum Distance Travelled* and the *Space Required*, the end result is a simulation of a buildfactory.

Maximum Distance Travelled

Algorithm 5: FACTORYADDTILE$(n_c, \mathbf{b}, m, C, c, w)$.

1: $\{\mathbf{hopper}\} \leftarrow$ HOPPER (c, n_c, w)
2: **if** $m = d$ **and** $\left(C_x \leq \max \mathbf{b}_x \text{ or } C_y < \min \mathbf{b}_y\right)$ **then**
3: $\{\mathbf{A}, \mathbf{b}\} \leftarrow$ DOWNDIR $(\mathbf{hopper}, \mathbf{b}, \mathbf{C})$
4: **else if** $m = l$ **and** $(C_y \leq \max \mathbf{b}_y$ **or** $C_x > \max \mathbf{b}_x)$ **then**
5: $\{\mathbf{A}, \mathbf{b}\} \leftarrow$ LEFTDIR $(\mathbf{hopper}, \mathbf{b}, \mathbf{C})$
6: **else if** $m = l$ **and** $(C_x \geq \max \mathbf{b}_x$ **or** $C_y > \max \mathbf{b}_y)$ **then**
7: $\{\mathbf{A}, \mathbf{b}\} \leftarrow$ UPDIR $(\mathbf{hopper}, \mathbf{b}, \mathbf{C})$
8: **else if** $m = r$ **and** $(C_y \geq \min \mathbf{b}_y$ **or** $C_x < \min \mathbf{b}_x)$ **then**
9: $\{\mathbf{A}, \mathbf{b}\} \leftarrow$ RIGHTDIR $(\mathbf{hopper}, \mathbf{b}, \mathbf{C})$
10: **return** $\{\mathbf{A}, \mathbf{b}\}$

Figure 2.14. Algorithm 5: Factory Add Tile [27].

Running a factory simulation has three phases: ramp up, production, and wind down. During the $n-1$ *ramp up* cycles, the first polyomino is being constructed one tile at a time and no polyominoes are produced. Clever design of delays in the part hoppers ensures no unconnected tiles are released. During *production cycles*, one polyomino is finished each cycle. Once the first part hopper empties, the $n-1$ *wind down* cycles each produce a complete polyomino as each successive hopper empties. This section analyzes maximum distance, defined as the maximum distance any tile must move. There are two results, *construction distance*, the maximum distance required to assemble a single polyomino from scratch, and *cycle distance*, the maximum distance required during production cycles to advance all partial assemblies one cycle. Since a polyomino contains n tiles, the *construction distance* during production cycles is $n \cdot$ (*cycle distance*).

Cycle distance is the sum of the maximum distances moved in each direction. As shown in figure 2.15a, polyominoes shaped as a n x *1* row require the longest distance of $4n + 16$. Polyominoes shaped as a 1 x n column requires the least distance of $2n + 16$. Construction distance therefore requires $O(\ n^2)$ distance.

Space Required

The space required by a factory is a function of the widths of individual sub-factories and height of the last sub-factory. The first sub-factory is constructed separately and it does not have any delay. Beginning from the second sub-factory, height can be computed as a function of the number of copies n_c of the polyomino, width of the hopper w, position of the sub-factory i, and rows of the sub-assembled polyomino $\mathbf{b}_y$ as in (2.8). If a tile is added before the top row of $\mathbf{b}$, then an additional row is added to the height. The width of the sub-factory can be calculated similarly as in (2.9) and (2.10). In a case where twice of $\mathbf{b}_x$ is greater than $width_{hopper+delays}$ then additional columns are added to the left of the sub-factory. When a tile is added to $\mathbf{b}$ using a down move, width also depends on the location of the column, $column_{loc}$, to which the tile is added.

$$height(i) = \lceil \frac{n_c}{w} \rceil + 2(\lceil \frac{i}{2} \rceil + \mathbf{b}_y) + \{4, for\ m = l\ or\ d, i \geq 2; \quad 7, for\ m = u\ or\ r, i \geq 2 \quad (2.8)$$

$$width_{hopper+delays} = w + 2\lceil \frac{i}{2} \rceil + 8,\ i \geq 2 \quad (2.9)$$

$$width(i) = width_{hopper+delays} + \{b_x - column_{loc}, for\ m = d; \quad 0,\ for\ m \neq d \quad (2.10)$$

Because a factory requires $O(n)$ rows and $O(n)$ columns, the total required space is $O(n^2)$. As shown in figure 2.15b, the required size is upper bounded by column-shaped

polyominoes and lower bounded by row-shaped polyominoes, and is $O(n^2)$.

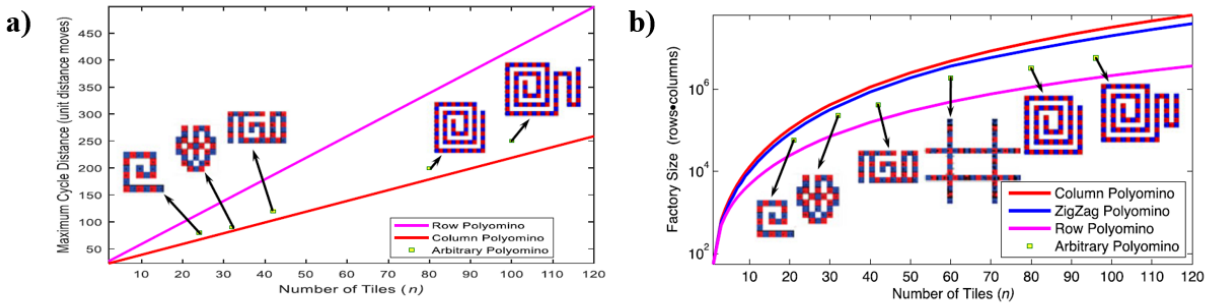

Figure 2.15. a) Worst-case cycle distance plotted as a function of polyomino size n.The cycle distance is the sum of distances to move during the r, d, l, u moves each cycle. Cycle distance increases linearly with polyomino size and is upper bounded by row parts and lower bounded by column parts. Total construction distance for a particle is n·cycle distance. b) Factory size grows quadratically with the number of tiles. [27]

From these Algorithms, a square shape from 4 polyominoes was simulated. From this simulation a microchannel system was then fabricated to test the validity of the algorithms of object particle computation under parallel global inputs. The simulated system is shown in figure 2.16(a-c), below.

On a 2in silicon wafer, this 4 Polyomino Algorithm was produced. After bringing the design into AutoCAD, the algorithm was then fabricated into a film mask (CAD/Art Services, Brandon OR, USA) for microfabrication purposes. The thickness of the microfludic channels were approximately 300μm and individual channels were approximately 300μm in width. The channel was fabricated using SU-8 2150 and used contact exposure to produce the pattern, after development, the channel was cleaned and ready for experimentation. The final product is shown in figure 2.16(d).

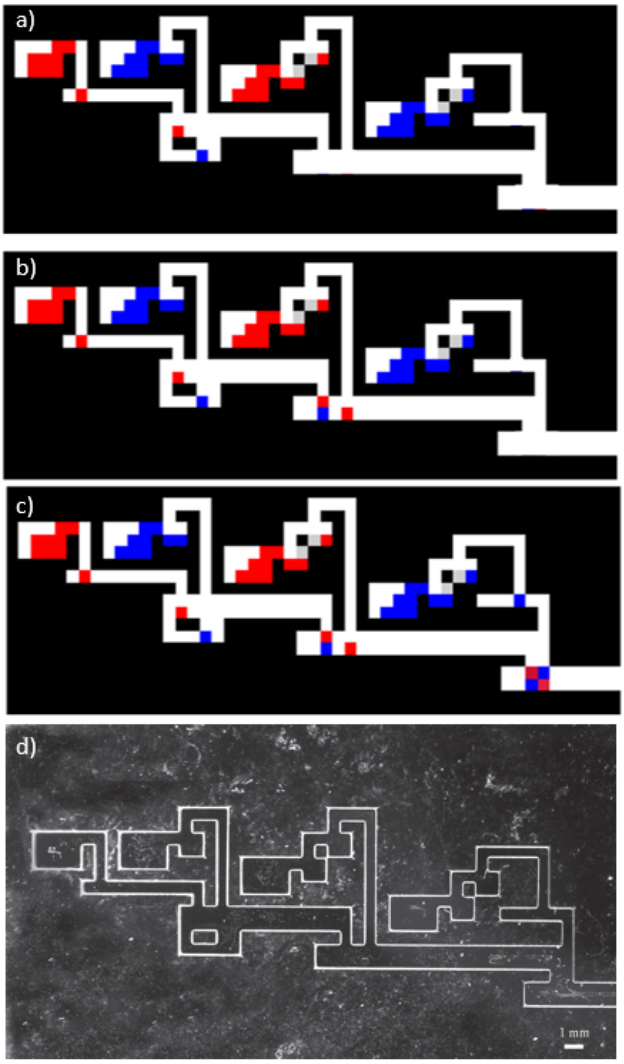

Figure 2.16. 4 Polyomino Square Algorithm. a) Algorithm after 6 inputs have been made into the system. b) Continued input leads to the fabrication of sub-polyomino microassembly. c) Final polyomino microassembly is shown in the bottom right corner. (Image Courtesy of Dr. Aaron Becker and Sheryl Manzoor). d) The microfludic channel device of a 4-polyomino square after microfabrication thickness of channels is approximately 300μm.

2.7. Experimental setup

When completing experiments with the Permanent Magnet Stage (PMS), the experimental setup described here was used. Experiments were conducted under a Zeiss Stemi 2000-C Stereoscopic Microscope. The experimental images were observed through a Motion Pro X3 camera. All images were captured at a frame rate of 30 fps. Figure 2.17 shows the experimental setup. From the initial inputs from the C++ program, the Arduino R3 relays the information to the stepper motor drivers. The control inputs passed through the drivers every 0.5 seconds. Thus, the permanent magnet moved with a velocity of 150 μm/s. The experimental chamber was made of Polydimethylsiloxane (PDMS), a 35mm petri dish, or a microfluidic device. The chamber was filled with a solution of Tween 20 and Deionized Water.

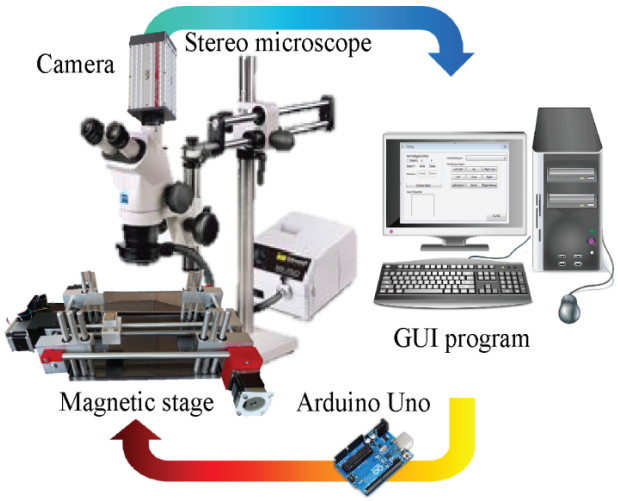

Figure 2.17. Experimental Setup [46]

Chapter 3

RESULTS AND DISCUSSION

3.1. Single Motion Manipulation

Actuation of the stage controller can show that the manufactured microrobots can be fully controllable. Initial commands began with a sequence of <up, right, down, left >, the alginate microrobots began to move as the magnet moved underneath. The initial position of the alginate microrobot was manipulated to create a box. In this experiment, the interaction of one singular alginate microrobot was demonstrated to show the ability to overcome the drag force using the magnetic field of a permanent magnet. Still, overcoming the drag of the alginate microrobot proved to be an individual challenge and required play with the control scheme of the permanent magnet location.

The permanent magnet was initially placed in the center of the field of view. At this point the alginate microrobot would not move. As the initial command was given the permanent magnet would move <up >, as the magnet moved over the alginate microrobot, the microrobot would not move until the trailing dipole of the magnet moved underneath. Following the magnets trailing dipole, the alginate microrobot moves to its destination. To allow the alginate microrobot to stop, the permanent magnet moves, in this case, <down >to the center of the microrobot. Through manipulation, where the magnet moves through the field of play with a velocity of 150 μm/s, a distance is created between the magnet and alginate microrobot, as such the alginate microrobot followed the permanent magnet with a varied mobility. In Fig. 3.1(a)-(c), a single alginate microrobot of 300 μm in diameter was manipulated to spell SMU. Due to the limited input direction, the heading angle for the

motion of aglginate microrobot is not varied.

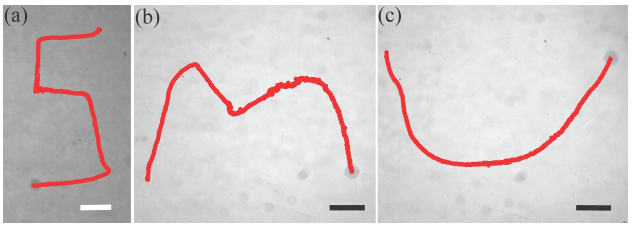

Figure 3.1. Resultant trajectories of a single alginate microrobot using manual control. (a) S trajectory during s, (b) M trajectory during 109 s, (c) U trajectory during 61 s. The scale bar represents 1 mm [46].

3.2. Swarm Motion Manipulation

Using the suggested magnetic stage controller, it is available to move multiple alginate microrobots and they swarm as a group. In order to swarm, the randomly distributed alginate microrobots need to be gathered as a group. The alginate microrobots in this experiment are approximately 300 μm in diameter. In the experiment, the separately located microrobots were illustrated in Fig. 3.2(a). Then, we located the permanent magnet at the A position and the separately located individual microrobot were gathered around the A position as shown in Fig. 3.2(b). The alginate microrobots were attracted by the magnetic field from the permanent magnet.

However, the alginate microrobot had less attracted force because of the long distance from the permanent magnet. Thus, the permanent magnet was moved to the B position in order to put those alginate microrobots close to the magnet. As a result, the most alginate microrobots were gathered around the B position as indicated in Fig. 3.2(d). As the magnet moved around the boundary of field, it will help gather all microrobot since the magnet can be of a strong magnetic field area.

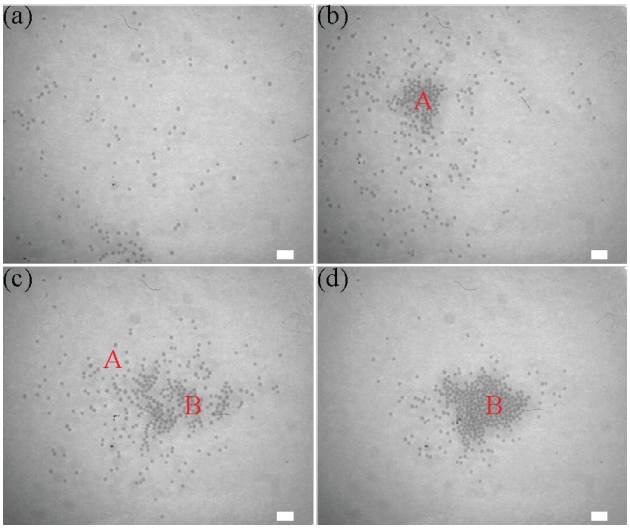

Figure 3.2. Aggregation motion for swarming group of alginate microrobots. (a) Initial distribution of each alginate microrobot at 0 s, (b) The instant motion when the permanent magnet was located at A position during 34 s, (c) The resultant location of alginate microrobots when the magnet was relocated the B position after 45 s passed from (b), (d) The final location of all microrobots after 28 s. The scale bar represents 1 mm [46].

Once the microrobots were gathered at the certain location, we made a swarm motion by moving the magnet. In Fig. 3.3(a), the more than 100 alginate microrobots were positioned at the left side. After the magnet moved toward the right side, they followed the magnet movement as shown in Fig. 3.3(b). As seen in Fig. 3.3, the drag forces of the alginate microrobots can be an issue at times. The trailing alginate microrobots of the swarm can be seen to have moved very little from the initial location of 0 s.

Following the experiments with alginate microrobot swarms, an additional task of moving a singular object was perused. In this experiment, the diameter size of the alginate microrobots are 300 μm. Using a 2.6 2.7 mm piece of PDMS, the alginate microrobots were then manipulated to move from their initial position seen in Fig. 3.4(a), as the magnet was moved from this position to is final position, the microrobots moved underneath of the PDMS piece. The some microrobots were in contact with the piece as the flow moved it across the field of

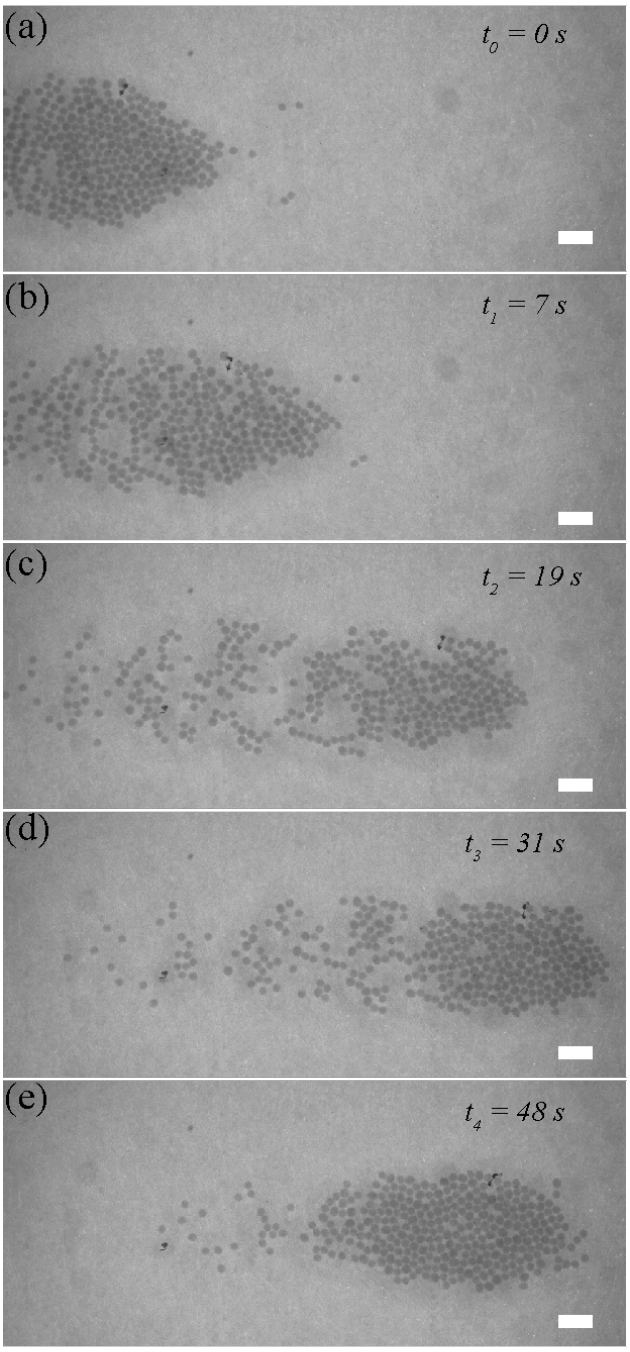

Figure 3.3. Translational swarming motion of alginate microrobots. (a) Initial positions of a swarming group at 0 s, The permanent magnet headed toward the right side forward the front of alginate microrobots and the motion was shown at (b), (c), (d), and (e). The scale bar represents 1mm [46].

view. Figure 3.4(d) shows the final position of the piece. The total distance the PDMS piece moved was 7.6 mm, over a 34 s span. This experiment result indicates that the swarming alginate microrobot are available to do microscale transportation task in the low Reynolds number.

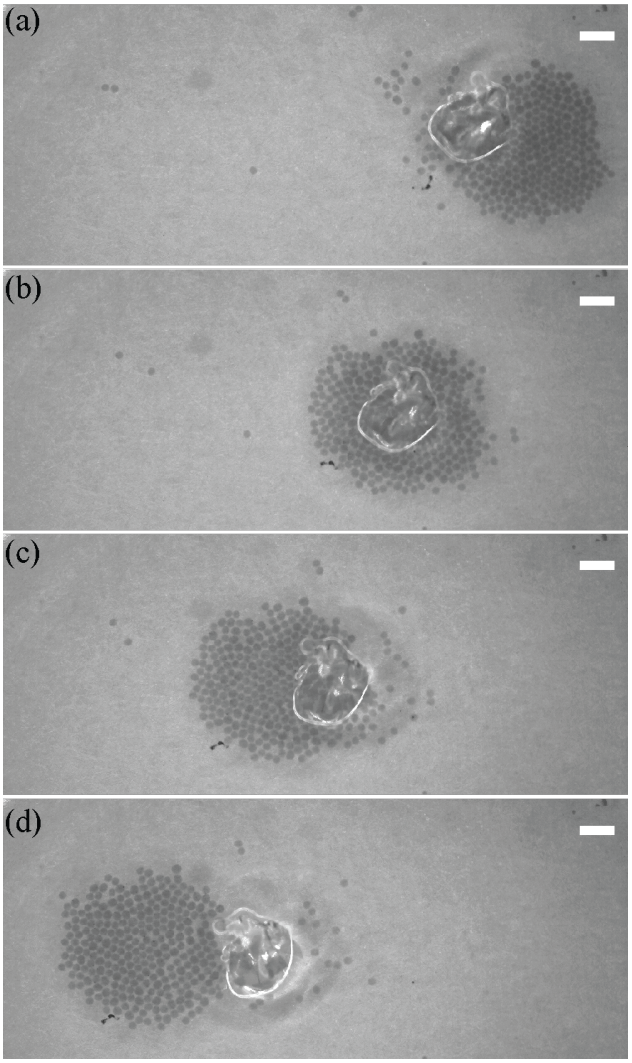

Figure 3.4. Transport task using swarming alginate microrobots. (a) Initial positions of a swarming group and a PDMS chunk(0 s), (b) Transport task motion at 16 s, (c) Transport task motion at 25 s, (d) Transport task motion at 34 s. The scale bar represents 1mm [46].

3.3. Object Particle Computation

With the microfludic factory network described in previously, undetermed, alginate microrobots were transported at each hopper, by way of a pipette. To show the process, one alginate particle was loaded in each hopper. The experimental channel was placed at the center of the stage. The magnet centered beneath the microfluidic factory layout. This position was saved as the home position for the permanent magnet. Stepper motors controlled the stage position. An Arduino UNO programmed in C++ commanded these step-per motors using a 2 Hz control loop. After a command was initiated, such as each direction in the <u, r, d, l >sequence, the permanent magnet was returned to the home position to better control the distribution of the magnetic gradient. The layout was observed through a stereomicroscope and the installed camera (Motion Pro X3) captured the procedure at 30 fps. Using 0.65x magnification in the stereomicroscope, the observed field of view is 23.6 x 18.9 mm^2.

Using a factory layout generated by a 4-polyomino square, we demonstrated micro-scale assembly using multiple alginate microrobots, the average microrobot diameter was 300 μm. 4-polyonimo square algorithm is shown in figure 3.5(a), the system shows the completion of square polyominoes. The initial scene in the microscale is shown in Fig. 3.5(a). The first assembly operation was then orchestrated by moving the magnet in a clockwise direction, following the <u, r, d, l >sequence as indicated in Fig. 3.5(b-d). Each input was applied sufficiently long to ensure all alginate microrobots touched a wall. Completion of the polyomino is shown in Fig. 3.5(e).

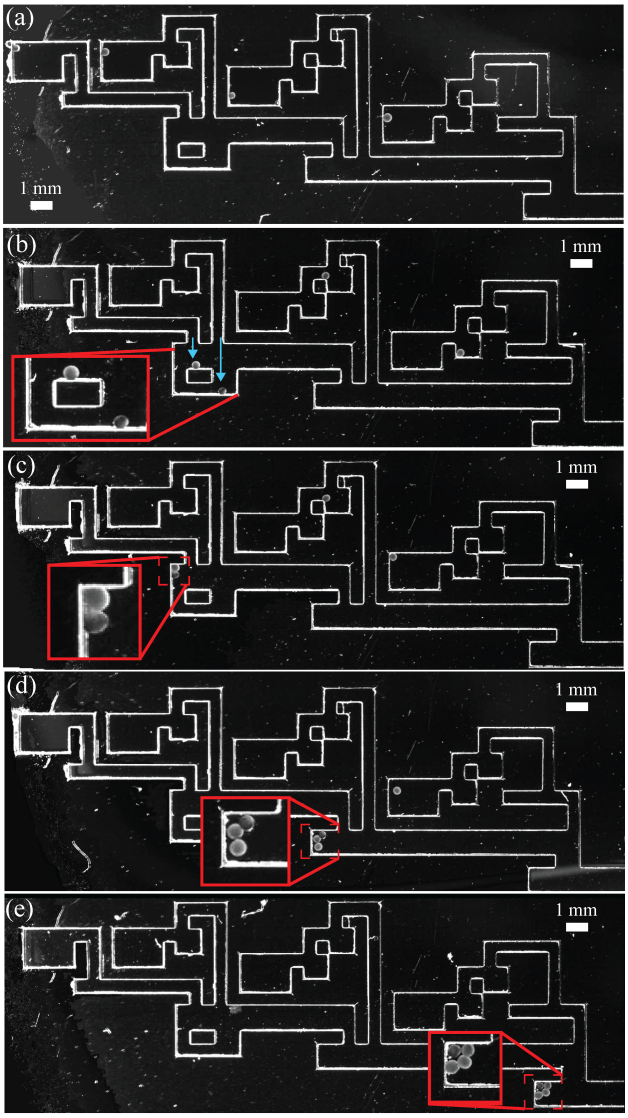

Figure 3.5. Showing the experimental results of ALG 4. (a) shows the individual alginate in its initial position. (b) After initial movements of the <u,r,d,l >, the alginate microrobots move to the position shown. (c) After <l,u >inputs are put into the system to produce the first multi-microrobot polyomino. (d) Shows the next three microrobot polyomino after applying multiple <u,r,d,l>sequences. (e) After the alginate microrobots have moved through the microfluidic factory layout, final product of the 4 polyomino algorithm is shown [27].

Chapter 4

DISCUSSION AND FUTURE WORK

4.1. Discussion

This work has shown the successful manipulation of single and swarms of alginate artificial cell soft-microrobots while using the permanent magnet stage. Individual and swarm manipulation showed the capacities to conduct specific tasks. Single microrobots were made to spell out SMU, disperesed particles were shown to aggregate and move sufficiently in swarms. The swarms were then made to move left to right and remained in a grouping throughout actuation with some breaking away from the cluster. Additionally, the task to move a single piece was PDMS was completed successfully. The successful 4 square polyomino microassembly was completed using the permanent magnet stage, this was done by moving the the permanent magnet in a clockwise direction and moving in the <u, r, d, l >motion as described in the rules of object particle computation for parallel assemblies.

4.2. Future Work

Further development is needed in the robustness of the microfluidic environment for the object particle computation. Investigation into this process has begun and a new microfluidic system has been fabricated with a rail system, as to reduce surface friction direction on the one contact point and help assist the particle as it moves through the system. Work in improving the PMS for autonomous control is also being investigated, as well as adding an additional motor specifically to rotate the permanent magnet. Rotation of the permanent magnet will allow the PMS to have rolling motion manipulation as well as dragging

manipulation. Additionally, development of artificial cell biosensing capabilities, such as the encapsulation of gold nanorods to sense the change in temperature and cause controlled deformations in the particle.

Appendix A

Published Works

Journal Papers

Manzoor, S., Sheckman, S., Lonsford, J., Kim, H., Kim, M.J., Becker, A.

Parallel Self-Assembly of Polyominoes under Uniform Control Inputs

IEEE Robotics and Automation Letters, 2017.

Ali, J., Cheang, U., Liu, Y., Kim, H., Rogowski, L., Sheckman, S., Patel, P., Sun, W., Kim, M.J.

Fabrication and Magnetic Control of Alginate-based Soft-microrobots

APL, 2016.

Conference Papers

Zhang, X., Kim, H., Rogowski, L., Sheckman, S., Kim, M.J.

Development and Implementation of 3D hexapole magnetic tweezer system for micromanipulations

The IEEE International Conference on Robotics and Automation (ICRA), 2018

Manzoor, S., Sheckman, S., Lonsford, J., Kim, H., Kim, M.J., Becker, A.

Parallel Self-Assembly of Polyominoes under Uniform Control Inputs

IEEE/RSJ International Conference on Intelligent Robots and Systems (IROS), 2017.

Sheckman, S., Kim, H. Manzoor, S., Rogowski, L., Huang, L., Zhang, X., Becker, A., Kim, M.J.

Manipulation and Control of Microrobots Using A Novel Permanent Magnet Stage

KROS Conference of Ubiquitous Robots and Ambient Intelligence (URAI), 2017

Sheckman, S., Kim, H. Manzoor, S., Rogowski, L., Huang, L., Zhang, X., Leclerc, J., Becker, A., Kim, M.J.

Manipulation of Alginate Microrobots by Permanent Magnet Stage

IEEE Manipulation, Automation and Robotics at Small Scales (MARSS), 2017.

Zhang, X., Kim, H., Rogowski, L., Sheckman, S., Kim, M.J.

Novel 3D Magnetic Tweezer System for Microswimmer Manipulations

KROS Conference of Ubiquitous Robots and Ambient Intelligence (URAI), 2017

Rogowski, L., Zhang, X., Kim, H., Sheckman, S., Kim, D., Kim, M.J.

Swimming in Synthetic Muscin

KROS Conference of Ubiquitous Robots and Ambient Intelligence (URAI), 2017

BIBLIOGRAPHY

[1] Abbott, J. J., Nagy, Z., Beyeler, F., and Nelson, B. J. Robotics in the small, part i: microbotics. *IEEE Robotics & Automation Magazine 14*, 2 (2007), 92–103. 1

[2] Ali, J., Cheang, U. K., Liu, Y., Kim, H., Rogowski, L., Sheckman, S., Patel, P., Sun, W., and Kim, M. J. Fabrication and magnetic control of alginate-based rolling microrobots. *AIP Advances 6*, 12 (2016), 125205. 3, 8

[3] Augustsson, P., Persson, J., Ekström, S., Ohlin, M., and Laurell, T. Decomplexing biofluids using microchip based acoustophoresis. *Lab on a Chip 9*, 6 (2009), 810–818. 4

[4] Becker, A., Demaine, E. D., Fekete, S. P., Habibi, G., and McLurkin, J. Reconfiguring massive particle swarms with limited, global control. In *International Symposium on Algorithms and Experiments for Sensor Systems, Wireless Networks and Distributed Robotics* (2013), Springer, pp. 51–66. 2, 4, 16

[5] Becker, A., Demaine, E. D., Fekete, S. P., and McLurkin, J. Particle computation: Designing worlds to control robot swarms with only global signals. In *Robotics and Automation (ICRA), 2014 IEEE International Conference on* (2014), IEEE, pp. 6751–6756. 2, 4, 16, 21

[6] Becker, A., Habibi, G., Werfel, J., Rubenstein, M., and McLurkin, J. Massive uniform manipulation: Controlling large populations of simple robots with a common input signal. In *Intelligent Robots and Systems (IROS), 2013 IEEE/RSJ International Conference on* (2013), IEEE, pp. 520–527. 4

[7] Castillo, J., Dimaki, M., and Svendsen, W. E. Manipulation of biological samples using micro and nano techniques. *Integrative Biology 1*, 1 (2009), 30–42. 1

[8] Chang, T. M. S. Therapeutic applications of polymeric artificial cells. *Nature Reviews Drug Discovery 4*, 3 (2005), 221. 2

[9] Chang, T. M. S. *Artificial cells: biotechnology, nanomedicine, regenerative medicine, blood substitutes, bioencapsulation, and cell/stem cell therapy*, vol. 1. World Scientific, 2007. 2

[10] Cheang, U. K., and Kim, M. J. Fabrication and control of simple low reynolds number microswimmers. *Applied Physics Letters 109*, 3 (2016), 034101. 3

[11] Cheang, U. K., Roy, D., Lee, J. H., and Kim, M. J. Fabrication and magnetic control of bacteria-inspired robotic microswimmers. *Applied Physics Letters 97*, 21 (2010), 213704. 3

[12] Chiang, P.-T., Mielke, J., Godoy, J., Guerrero, J. M., Alemany, L. B., Villagomez, C. J., Saywell, A., Grill, L., and Tour, J. M. Toward a light-driven motorized nanocar: Synthesis and initial imaging of single molecules. *ACS nano 6*, 1 (2011), 592–597. 1

[13] Chiou, P. Y., Ohta, A. T., and Wu, M. C. Massively parallel manipulation of single cells and microparticles using optical images. *Nature 436*, 7049 (2005), 370. 4

[14] Chowdhury, S., Jing, W., and Cappelleri, D. J. Controlling multiple microrobots: recent progress and future challenges. *Journal of Micro-Bio Robotics 10*, 1-4 (2015), 1–11. 1

[15] De Lanauze, D., Felfoul, O., Turcot, J.-P., Mohammadi, M., and Martel, S. Three-dimensional remote aggregation and steering of magnetotactic bacteria microrobots for drug delivery applications. *The International Journal of Robotics Research 33*, 3 (2014), 359–374. 1

[16] Desai, J. P., Pillarisetti, A., and Brooks, A. D. Engineering approaches to biomanipulation. *Annu. Rev. Biomed. Eng. 9* (2007), 35–53. 4

[17] Diller, E., Giltinan, J., and Sitti, M. Independent control of multiple magnetic microrobots in three dimensions. *The International Journal of Robotics Research 32*, 5 (2013), 614–631. 1

[18] Donald, B. R., Levey, C. G., Paprotny, I., and Rus, D. Planning and control for microassembly of structures composed of stress-engineered mems microrobots. *The International journal of robotics research 32*, 2 (2013), 218–246. 1

[19] Gassner, A.-L., Abonnenc, M., Chen, H.-X., Morandini, J., Josserand, J., Rossier, J. S., Busnel, J.-M., and Girault, H. H. Magnetic forces produced by rectangular permanent magnets in static microsystems. *Lab on a Chip 9*, 16 (2009), 2356–2363. 13

[20] Haeberle, S., Naegele, L., Burger, R., Stetten, F. v., Zengerle, R., and Ducrée, J. Alginate bead fabrication and encapsulation of living cells under centrifugally induced artificial gravity conditions. *Journal of microencapsulation 25*, 4 (2008), 267–274. 9

[21] Jing, W., Pagano, N., and Cappelleri, D. J. A tumbling magnetic microrobot with flexible operating modes. In *Robotics and Automation (ICRA), 2013 IEEE International Conference on* (2013), IEEE, pp. 5514–5519. 1

[22] Kim, J., and Lee, S. Modeling drag force acting on the individual particles in low reynolds number flow. *Powder Technology 261* (2014), 22–32. 15

[23] Lin, Y.-H., Yang, Y.-W., Chen, Y.-D., Wang, S.-S., Chang, Y.-H., and Wu, M.-H. The application of an optically switched dielectrophoretic (odep) force for the manipulation and assembly of cell-encapsulating alginate microbeads in a microfluidic perfusion cell culture system for bottom-up tissue engineering. *Lab on a Chip 12*, 6 (2012), 1164–1173. 4

[24] Mahoney, A. W., and Abbott, J. J. Generating rotating magnetic fields with a single permanent magnet for propulsion of untethered magnetic devices in a lumen. *IEEE Transactions on Robotics 30*, 2 (2014), 411–420. 4

[25] Majidi, C. Soft robotics: a perspectivecurrent trends and prospects for the future. *Soft Robotics 1*, 1 (2014), 5–11. 1

[26] Manzoor, S., and Becker, A. Particle Assembly, 2017. 17

[27] Manzoor, S., Sheckman, S., Lonsford, J., Kim, H., Kim, M. J., and Becker, A. T. Parallel self-assembly of polyominoes under uniform control inputs. *IEEE Robotics and Automation Letters 2*, 4 (2017), 2040–2047. 16, 17, 18, 19, 20, 21, 22, 23, 24, 26, 35

[28] Martel, S., and Mohammadi, M. A robotic micro-assembly process inspired by the construction of the ancient pyramids and relying on several thousand flagellated bacteria acting as micro-workers. In *Intelligent Robots and Systems, 2009. IROS 2009. IEEE/RSJ International Conference on* (2009), IEEE, pp. 426–427. 1

[29] Mørch, Ý. A., Donati, I., Strand, B. L., and Skjåk-Bræk, G. Effect of ca2+, ba2+, and sr2+ on alginate microbeads. *Biomacromolecules 7*, 5 (2006), 1471–1480. 2, 6

[30] Motwani, S. K., Chopra, S., Talegaonkar, S., Kohli, K., Ahmad, F. J., and Khar, R. K. Chitosan–sodium alginate nanoparticles as submicroscopic reservoirs for ocular delivery: formulation, optimisation and in vitro characterisation. *European Journal of Pharmaceutics and Biopharmaceutics 68*, 3 (2008), 513–525. 2

[31] Nelson, B. J. Microrobotics in medicine. *ETH Zurich Institute of Robotics and Intelligent Systems, Tech. rep* (2006). 13

[32] Ou, Y., Kim, D. H., Kim, P., Kim, M. J., and Julius, A. A. Motion control of magnetized tetrahymena pyriformis cells by a magnetic field with model predictive control. *The International Journal of Robotics Research 32*, 1 (2013), 129–140. 1, 3

[33] Park, S. J., Lee, Y. K., Cho, S., Uthaman, S., Park, I.-K., Min, J.-J., Ko, S. Y., Park, J.-O., and Park, S. Effect of chitosan coating on a bacteria-based alginate microrobot. *Biotechnology and bioengineering 112*, 4 (2015), 769–776. 3

[34] Prakash, S. *Artificial cells, cell engineering and therapy*. Elsevier, 2007. 2

[35] Purcell, E. M. Life at low reynolds number. In *Physics and Our World: Reissue of the Proceedings of a Symposium in Honor of Victor F Weisskopf* (2014), World Scientific, pp. 47–67. 3

[36] Rashid, M. F. F., Hutabarat, W., and Tiwari, A. A review on assembly sequence planning and assembly line balancing optimisation using soft computing approaches. *The International Journal of Advanced Manufacturing Technology 59*, 1-4 (2012), 335–349. 5

[37] Rogowski, L. W., Kim, H., Zhang, X., Sheckman, S., Kim, D., and Kim, M. J. Swimming in synthetic mucus. In *Ubiquitous Robots and Ambient Intelligence (URAI), 2017 14th International Conference on* (2017), IEEE, pp. 512–516. 3

[38] Rubenstein, M., Ahler, C., and Nagpal, R. Kilobot: A low cost scalable robot system for collective behaviors. In *Robotics and Automation (ICRA), 2012 IEEE International Conference on* (2012), IEEE, pp. 3293–3298. 1

[39] Ryan, P., and Diller, E. Five-degree-of-freedom magnetic control of micro-robots using rotating permanent magnets. In *Robotics and Automation (ICRA), 2016 IEEE International Conference on* (2016), IEEE, pp. 1731–1736. 4

[40] Samudrala, N., Nam, J., Sarfati, R., Style, R. W., and Dufresne, E. R. Mechanical stability of particle-stabilized droplets under micropipette aspiration. *Physical Review E 95*, 1 (2017), 012805. 6

[41] Sarmento, B., Ferreira, D., Veiga, F., and Ribeiro, A. Characterization of insulin-loaded alginate nanoparticles produced by ionotropic pre-gelation through dsc and ftir studies. *Carbohydrate Polymers 66*, 1 (2006), 1–7. 2

[42] Sarmento, B., Ribeiro, A., Veiga, F., Ferreira, D., and Neufeld, R. Insulin-loaded nanoparticles are prepared by alginate ionotropic pre-gelation followed by chitosan polyelectrolyte complexation. *Journal of nanoscience and nanotechnology 7*, 8 (2007), 2833–2841. 2

[43] Sarmento, B., Ribeiro, A., Veiga, F., Sampaio, P., Neufeld, R., and Ferreira, D. Alginate/chitosan nanoparticles are effective for oral insulin delivery. *Pharmaceutical research 24*, 12 (2007), 2198–2206. 2

[44] Seol, Y.-J., Kang, H.-W., Lee, S. J., Atala, A., and Yoo, J. J. Bioprinting technology and its applications. *European Journal of Cardio-Thoracic Surgery 46*, 3 (2014), 342–348. 7

[45] Seymour, J., and Cappelleri, D. J. Automated microassembly sequence planning with sub-assemblies. In *ASME 2016 International Design Engineering Technical Conferences and Computers and Information in Engineering Conference* (2016), American Society of Mechanical Engineers, pp. V004T08A018–V004T08A018. 4

[46] Sheckman, S., Kim, H., Manzoor, S., Rogowski, L. W., Huang, L., Zhang, X., Becker, A. T., and Kim, M. J. Manipulation and control of microrobots using a novel permanent magnet stage. In *Ubiquitous Robots and Ambient Intelligence (URAI), 2017 14th International Conference on* (2017), IEEE, pp. 692–696. 9, 11, 28, 30, 31, 32, 33

[47] Shields IV, C. W., Reyes, C. D., and López, G. P. Microfluidic cell sorting: a review of the advances in the separation of cells from debulking to rare cell isolation. *Lab on a Chip 15*, 5 (2015), 1230–1249. 4

[48] Sitti, M., Ceylan, H., Hu, W., Giltinan, J., Turan, M., Yim, S., and Diller, E. Biomedical applications of untethered mobile milli/microrobots. *Proceedings of the IEEE 103*, 2 (2015), 205–224. 1

[49] Su, Q. Computer aided geometric feasible assembly sequence planning and optimizing. *The International Journal of Advanced Manufacturing Technology 33*, 1-2 (2007), 48–57. 5

[50] Tabatabaei, S. N., Lapointe, J., and Martel, S. Hydrogel encapsulated magnetic nanoparticles as hyperthermic actuators for microrobots designed to operate in the vascular network. In *Intelligent Robots and Systems, 2009. IROS 2009. IEEE/RSJ International Conference on* (2009), IEEE, pp. 546–551. 2

[51] Tasoglu, S., Diller, E., Guven, S., Sitti, M., and Demirci, U. Untethered micro-robotic coding of three-dimensional material composition. *Nature communications 5* (2014), 3124. 4

[52] Tasoglu, S., Yu, C., Gungordu, H., Guven, S., Vural, T., and Demirci, U. Guided and magnetic self-assembly of tunable magnetoceptive gels. *Nature communications 5* (2014), 4702. 4

[53] Tavakoli, J., and Tang, Y. Hydrogel based sensors for biomedical applications: An updated review. *Polymers 9*, 8 (2017), 364. 2

[54] Trivedi, D., Rahn, C. D., Kier, W. M., and Walker, I. D. Soft robotics: Biological inspiration, state of the art, and future research. *Applied bionics and biomechanics 5*, 3 (2008), 99–117. 1

[55] Tung, H.-W., Maffioli, M., Frutiger, D. R., Sivaraman, K. M., Pané, S., and Nelson, B. J. Polymer-based wireless resonant magnetic microrobots. *IEEE Transactions on Robotics 30*, 1 (2014), 26–32. 1

[56] Vigolo, D., Rusconi, R., Stone, H. A., and Piazza, R. Thermophoresis: microfluidics characterization and separation. *Soft Matter 6*, 15 (2010), 3489–3493. 4

[57] Weibel, D. B., DiLuzio, W. R., and Whitesides, G. M. Microfabrication meets microbiology. *Nature Reviews Microbiology 5*, 3 (2007), 209. 1

[58] Yi, C., Li, C.-W., Ji, S., and Yang, M. Microfluidics technology for manipulation and analysis of biological cells. *Analytica Chimica Acta 560*, 1-2 (2006), 1–23. 1